

---

# Implicit Geometry and Interaction Embeddings Improve Few-Shot Molecular Property Prediction

---

Christopher Fifty<sup>\*,1</sup>, Joseph M. Paggi<sup>\*,1</sup>, Ehsan Amid<sup>2</sup>,  
Jure Leskovec<sup>1</sup>, Ron Dror<sup>1</sup>  
Equal Contribution<sup>\*</sup>  
Stanford University<sup>1</sup>, Google Brain<sup>2</sup>,  
fifty@cs.stanford.com

## Abstract

Few-shot learning is a promising approach to molecular property prediction as supervised data is often very limited. However, many important molecular properties depend on complex molecular characteristics — such as the various 3D geometries a molecule may adopt or the types of chemical interactions it can form — that are not explicitly encoded in the feature space and must be approximated from low amounts of data. Learning these characteristics can be difficult, especially for few-shot learning algorithms that are designed for fast adaptation to new tasks. In this work, we develop molecular embeddings that encode complex molecular characteristics to improve the performance of few-shot molecular property prediction. Our approach leverages large amounts of synthetic data, namely the results of molecular docking calculations, and a multi-task learning paradigm to structure the embedding space. On multiple molecular property prediction benchmarks, training from the embedding space substantially improves Multi-Task, MAML, and Prototypical Network few-shot learning performance. Our code is available at <https://github.com/cfifty/IGNITE>.

## 1 Introduction

In stark contrast to common applications in computer vision and natural language processing, little supervised data is available for many important molecular property prediction tasks [2, 36]. Determining the biological effects of a molecule—for example, a drug candidate—often involves a lengthy period of cell cultivation followed by a multi-step assay requiring specialized equipment [22]. Certain properties, such as toxicity, may even require animal studies to effectively measure [26]. The throughput of these assays and studies is limited, and synthesizing molecules to be tested is often expensive [6]. As a result, supervised datasets measuring molecular properties often contain on the order of 10s or 100s of data points, and few-shot learning algorithms are necessary to cope with the scarcity of labeled data [31].

Few-shot learning algorithms are designed for low-data paradigms, but the effectiveness of these approaches for molecular property prediction, such as the toxicity of a molecule or its binding affinity with a specific protein, is constrained by the inherent complexity of molecular interactions [9, 12]. Molecules are specified as a connected graph of atoms, each with its own feature vector, but this feature space does not directly encode complex molecular characteristics, such as the various 3D geometries a molecule may adopt or the types of chemical interactions it can form in each geometry [40]. These characteristics are essential to the real-world properties of molecules and deterministic of how molecules interact with other molecules, including proteins, enzymes, biological targets, and anti-targets [5].

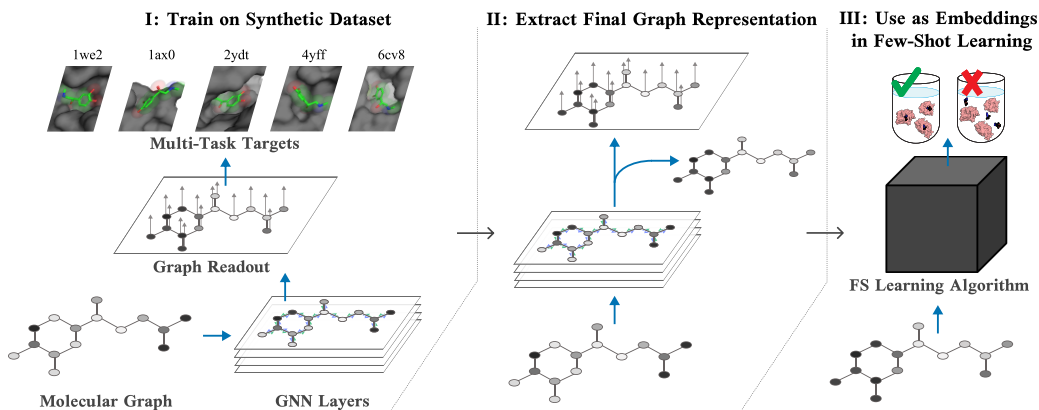


Figure 1: The end-to-end paradigm of developing of **IGNITE** embeddings: (I) train a multi-task GNN to map a small molecule to binding energies (kcal/mol) determined by the interactions between this small molecule and protein targets by physics-based docking. (II) extract the pre-readout graph representation. (III) for a few-shot learning algorithm, replace the default feature space with the learned molecular embeddings. The multi-task targets 1we2, 1ax0, 2ydt, 4yff, and 6cv8, represent Protein Data Bank codes for 5 of the 2,034 targets in our actual dataset.

While molecular representations encoding these attributes may be learned from the feature space, doing so injects an additional layer of complexity into the learning process. As the learning dynamics of few-shot learning algorithms are already quite complex — and sometimes even unstable [3] — training a model to develop both the capacity to rapidly adapt to new tasks as well as to approximate complex molecule-target interactions may be difficult, or even impossible, for existing algorithms.

In this work, we develop molecular embeddings that encode complex molecular characteristics to improve few-shot molecular property prediction. Our approach begins with curating a large-scale synthetic dataset that measures how 1,000s of molecules bind to each one of 1,000s of different proteins, therefore implicitly encoding the various 3D geometries a molecule may adopt as well as the chemical interactions it may form within the modeling objective of this dataset. We then train a MPNN [15] with a multi-task learning scheme—using a single model to predict the interactions among all molecules and targets—to learn a single molecular representation that generalizes to all tasks. Finally, we extract the final-layer learned representation of the multi-task MPNN as a molecular embedding, and use it to initialize the feature space of other few-shot learning algorithms on down-stream molecular property prediction tasks. This approach is visualized in Figure 1, and because of its ability to capture the implicit characteristics of a molecule, we call this method **Implicit Geometry aNd InTeraction Embedding (IGNITE)**.

In summary, our primary contribution is to develop molecular embeddings that implicitly encode the various 3D geometries a molecule can adopt and the types of chemical interactions it can form, much as word embeddings encode the potential meanings and usages of a word. Our analysis in Section 4 shows these characteristics are encoded into the embedding space, so that molecules with similar attributes are close together and molecules with different attributes are far apart. Further, on the FS-Mol and MoleculeNet molecular property prediction benchmark suites, with property predictions ranging from toxicity to inhibiting HIV replication, we find that **IGNITE** almost universally improves the performance of Multi-Task, MAML, and Prototypical Network few-shot learning algorithms. This improvement is somewhat remarkable as it is manifest without hyperparameter tuning and by simply modifying the input space upon which the few-shot learning methods operate.

## 2 Related Works

Significant effort has been devoted to addressing challenges associated with training few-shot learning models on small-scale molecular property prediction datasets. We partition these efforts into two collections. The first relates to developing new training objectives for self-supervised pre-training, while the second focuses on incorporating desirable domain-specific inductive biases into the learning process.

Self-supervised training approaches often aim to learn fundamental representations of small molecules sans labeled data. Many techniques apply a variation of atom, subgraph, or structural motif level masking and reconstruction [1, 17, 24, 28], while others begin to incorporate spatial information into molecular graphs to predict the distances among atoms [11, 19, 23, 42]. Still yet others adopt ideas

from contrastive learning: creating augmented views of molecular graphs and then learning graphical representations so that the similarity between different views of the same molecule is maximized while the similarity between views of different molecules is minimized [16, 37, 41, 43]. However, Sun et al. [32] finds self-supervised pre-training often conveys a negligible benefit and suggest much of the improvement attributed to self-supervised methods may be derived from extensive hyperparameter tuning of downstream tasks rather than the pre-training strategy itself.

A second perspective focuses on enhancing few-shot learning methodologies with inductive biases desirable for molecular machine learning. Wang et al. [35] propose using a molecule relation graph to improve few-shot learning performance. Schimunek et al. [29] encode context into molecular representations by querying Modern Hopfield Networks to replace a molecule’s representation with that of an associated context molecule, and Chen et al. [8] augment molecular meta-learning with an adaptive kernel fitting framework. Finally, Stanley et al. [31] adapts conventional few-shot learning baselines such as multi-task learning [7], model-agnostic meta-learning [13], and prototypical networks [30] to a robust few-shot learning molecular property prediction benchmark. Our findings in Section 5 suggest our approach may be complementary to these methods, simply transforming the feature space upon which they operate to an embedding space that is sensitive to complex molecular characteristics such as 3D geometry and chemical interaction.

### 3 IGNITE: Implicit Geometry and Interaction Embedding

While few-shot learning algorithms are designed for low-data paradigms, the effectiveness of these approaches can be limited by the inherent complexity of molecular interactions. We aim to improve their performance by changing the feature space upon which they operate to implicitly encode the various 3D geometries a molecule may adopt as well as the chemical interactions it may form in those geometries. The challenge is to learn an embedding that encodes this information.

**Synthetic Data Generation.** We may learn such an embedding by pre-training on a sufficiently large amount of data that relies upon 3D molecular geometries and chemical interactions. In principle, this data could be experimental measurements collected in a laboratory that quantify how small molecules bind to proteins. However in practice, experimental data on molecule-protein binding energy is limited, both in quantity and quality. Moreover, the measurements in this data come from a wide variety of different assays, from fluorescence-based functional screens to nuclear magnetic resonance experiments. Comparing the measurements from one assay type with another can be difficult, both for medicinal chemists as well as few-shot learning paradigms.

Instead, we turn to computational “docking” methods to generate synthetic data that encodes complex molecular characteristics. In particular, we use Glide, a physics-based docking program [14] to curate a large-scale synthetic dataset measuring how 1,000s of molecules bind to each of 1,000s of different proteins. Using such synthetic data has two key advantages. First, we can generate as much training data as we need. Second, it overcomes the difficulties in comparing experimental measurements across different assay types.

Given the 3D structure of a target protein and the chemical graph of a small molecule, docking methods estimate the binding energy between the two. Docking matches the process by which real binding energies arise in two key ways. First, docking considers many potential geometries of the protein–small molecule complex, including sampling over the potential internal 3D geometries of the small molecule, and the final prediction is related to the most favorable geometry found. Second, the favorability of each potential geometry is assessed using a physics-inspired scoring function quantifying the complementarity of molecular geometries and presence of key chemical interactions. We reason that pre-training on a sufficiently large amount of synthetic data generated by molecular docking would encode molecular attributes deterministic of their interactions into a model’s learned representations. To learn these representations, we turn to multi-task learning.

**Multi-Task Learning Paradigm.** The synthetic dataset naturally induces a multi-task learning paradigm where each protein represents a separate task. Specifically, for each protein target, we map a small molecule input to its binding energy (kcal/mol) as determined by molecular docking. This process is then repeated across the 1,000s of protein targets in our dataset to compose a multi-task learning system that uses a single deep learning model to predict how a small molecule will bind to any of the proteins in our dataset.

With regard to the model itself, we use a 10-layer MPNN [15] augmented with PNA [10] and using a graph readout composed of an element-wise maximum, learned multi-headed weighted sum, and learned multi-headed weighted mean. Each layer in the MPNN uses a Pre-Norm [39] transformer-like [34] residual structure with ReZero weighing [4] using a vector formulation as described in [33]. Moreover, a BOOM-layer [25] is used for a second residual connection after message-passing. The post-readout molecular representation is then passed through a shallow MLP that is shared among all tasks before a task-specific linear projection is used to predict the binding energy.

Our optimization protocol uses a linear warmup schedule with 100 steps and Adam [21] optimizer. The objective function is to minimize the mean squared error between the model’s predictions and the free energy measurements. We randomly split our synthetic dataset into 80% train and 20% validation, and use early stopping with a window size of 10 epochs on the validation dataset. Training spans 100 epochs, we save the best model checkpoint from early stopping to disk.

**Usage in Few-Shot Learning.** Many few-shot learning algorithms for molecular property operate on a connected graph of atom-level feature vectors. Atom-level feature vectors often include a one-hot encoding of the element type, atomic charge, mass, valency, etc. With **IGNITE**, we simply change the feature space on which few-shot learning algorithms operate from the default featurization—using a one-hot encoding of element type, atomic charge, etc.—to the pre-readout atom representation learned on the synthetic dataset by predicting binding energies.

To summarize, **IGNITE** pre-trains a multi-task model on large-scale synthetic dataset that implicitly encodes complex molecular characteristics—such as the various 3D geometries a molecule may adopt as well as the chemical interactions it may form—within its modeling objective. It then exports the final MPNN layer’s output representation, a connected graph of atom-level learned embeddings, to initialize the feature space of a few-shot learning algorithm. This approach is visualized in Figure 1, and our empirical findings in Section 5 suggests it can substantively boost few-shot learning performance.

## 4 IGNITE Analysis

While our MPNN model may fit the docking data, it is unclear if relevant biophysical knowledge is actually encoded into the learned **IGNITE** embeddings. Answering this question is the focus of our analysis.

### 4.1 Molecular Space Analysis

Our analysis commences with an exploration of various molecular spaces, and how the molecular space structure implicitly defines a notion of similarity among molecules within that space. We present 3 ways to measure distance between molecules: docking-based, embedding-based, and fingerprint-based. Later, we use the notion of distance among molecules—distance being a proxy for similarity—to quantify if the molecular characteristics implicitly captured by molecular docking are encoded into the **IGNITE** embedding space. We employ the Kendall Tau measure [20] to objectively quantify this effect.

**Docking-Based Distance.** Physics-based docking software implicitly encodes a notion of similarity among small molecules. For instance, one may define “similar” small molecules as those that manifest similar binding energies across many different protein targets; such molecules typically adopt similar 3D conformations and form similar chemical interactions with the same target. We quantify the implicitly defined similarity between a pair of molecules  $m_1, m_2$  from docking as the relative difference in docking energies across all targets:

$$d(m_1, m_2) = \sum_{t \in \text{targets}} \frac{|t(m_1) - t(m_2)|}{\max_m \{t(m)\} - \min_m \{t(m)\}}. \quad (1)$$

We compute the relative difference in binding energy as opposed to the absolute difference as different targets have different ranges of binding energies, and we wish to avoid lending more weight to targets with larger ranges than to targets with smaller ranges.

**Embedding-Based Distance.** Next we define the distance between molecules in the **IGNITE** embedding space. Our MPNN embedding model uses a combined graph readout composed of an element-wise max, learned weighted sums, and learned weighted means. Applying any of these

pooling operations to the per-atom **IGNITE** embeddings will output a component of the vector used to predict the binding energies associated with this target. Accordingly, we choose the simplest operation — element-wise max pooling — to motivate the distance between two arbitrary molecules in our embedding space.

Let  $m_1, m_2$  be two molecules parameterized by a per-atom, learned feature matrix and an adjacency matrix in the embedding space:  $m_1^{(e)} = (\mathcal{V}_1^{(e)}, \mathcal{E}_1^{(e)})$ . We define  $\rho$  to be the max-pooling operation across the embedding dimension for all nodes in the graph.

$$\text{For atom embeddings } \mathcal{V}^{(e)} = \begin{bmatrix} v_{1,1} & \dots & v_{1,d} \\ \dots & & \\ v_{n,1} & \dots & v_{n,d} \end{bmatrix} \in \mathbb{R}^{n \times d},$$

$$\rho(\mathcal{V}^{(e)}) \in \mathbb{R}^d, \text{ where } [\rho(\mathcal{V}^{(e)})]_j = \max_i v_{ij}.$$

We can now define the distance between two molecules in the embedding space as the  $l_2$  norm of their element-wise maximum difference:

$$d_\rho(m_1, m_2) = \|\rho(\mathcal{V}_1) - \rho(\mathcal{V}_2)\|_2 \quad (2)$$

One may also apply Equation 2 to the initial feature space used as input to the model:

$$m_1^{(f)} = (\mathcal{V}_1^{(f)}, \mathcal{E}_1^{(f)})$$

A model’s feature space is simply the initial numerical representation of a molecule. Machine learning models often define an atom-level feature space as a numerical vector encoding an atom’s element type atomic charge, atomic mass, valency and/or other atomic-level quantities.

**Fingerprint-Based Distance.** A third metric of the distance between two molecules is the Tanimoto distance  $d_\tau$  between their extended-connectivity fingerprints (ECFPs). An ECFP is a binary string indicating whether or not each of many 2D chemical substructures is present in a given molecule. This Tanimoto distance—which is one of the most commonly used notions of molecular similarity in both academia and industry [27]—is defined as the number of chemical sub-structures shared between a pair of molecules divided by the total number of chemical sub-structures present in either molecule. A high value indicates that a pair of molecules share the same components but does not necessarily indicate that those components are connected to one another in the same way or positioned similarly in 3D space.

**Kendall Tau Measure.** While one may define various metrics to determine the distance among molecules within a molecular space, comparing distances across molecular spaces is more involved. One may abstract the notion of distance between two pairs of molecules to an ordering of all molecules ranked by distance to a single anchor molecule. By ranking the similarity of all molecules to an anchor molecule in one molecular space, we may quantify the extent to which other molecular spaces produce a (dis)similar ordering with respect to this same anchor molecule.

We employ the Kendall Tau rank distance [20], also known as the bubble-sort distance, to quantify how similar one ranking of molecular similarity is to the docking-based ordering induced by Equation 1. The Kendall Tau rank distance is given by:

$$K_d(\tau_1, \tau_2) = |(i, j) : i < j, \{[\tau_1(i) \wedge \tau_2(i) > \tau_2(j)] \\ \vee [\tau_1(i) > \tau_1(j) \wedge \tau_2(i) < \tau_2(j)]\}|$$

where  $\tau_1(i)$  and  $\tau_2(i)$  are the rankings of molecule  $i$  given by the rankings  $\tau_1$  and  $\tau_2$ , respectively. Intuitively, Kendall Tau counts the number of swaps made during a bubble sort to convert the ordering in the **IGNITE** embedding space, feature space, or ECFP space to the ordering in the docking space. The smaller the Kendall Tau distance between two molecular spaces with respect to the same anchor molecule, the more “similar” they are in the sense of molecular space structure with relation to that anchor molecule.

**Findings.** A naïve Kendall Tau analysis would compare the product space of space of  $(32,547 \times 32,547)$ , with each unique molecule in our synthetic dataset serving as an anchor molecule for all other molecules. As this comparison exceeds our computational resources, we randomly sample 100 anchor molecules instead to compare the relative orderings induced by various molecule spaces with

the ordering induced by the docking-based distance in Equation 1. This analysis approximates how “similar” the various molecular spaces are to the docking-based space, the space that directly encodes the various 3D geometries a molecule may adopt as well as the chemical interactions it can form.

Our findings are summarized in Table 1 and indicate ranking molecules by distance in the **IGNITE** embedding space is most similar to the rankings induced by distance in the docking space. Orderings among molecules in ECFP space requires, on average, 4.5 million more swaps than orderings in the **IGNITE** embedding space. Similarly, the feature space requires 77 million more swaps to reorder its structure to match the docking-space than does the **IGNITE** embedding space. The “Random” entry in Table 1 represents a randomly structured molecular space and serves as a reference value for comparison.

Table 1: Kendall Tau Analysis. Scores are averaged across 100 randomly selected small molecules. The number of swaps indicates the average number of swaps made by KT to transform an ordering to the docking-based ordering. Normalized Kendall Tau is the number of swaps divided by the number of molecules in an ordering.

Molecular Space	Number of Swaps (↓)	Normalized Kendall Tau (↓)
Docking	0	0
<b>IGNITE</b>	$2.96 \times 10^7$	0.386
Feature	$3.73 \times 10^7$	0.488
ECFP	$3.28 \times 10^7$	0.429
Random	$3.83 \times 10^7$	0.50

## 4.2 Visualized Example

To supplement our quantitative analysis, we offer qualitative analysis of two small molecules that have dissimilar 2D chemical structures, but are known to adopt similar 3D conformations when binding to a biological target. We select CHEMBL200234 and levisoprenaline as the small molecules and the  $\beta_1$ -adrenergic receptor (B1AR) as the protein target. While these two molecules are chemically very different, as seen in Figure 2, examining the experimentally determined structure of each one bound to B1AR reveals they adopt similar 3D conformations and form similar chemical interactions (e.g., hydrogen bonds) with the target.

It would be expected that Tanimoto distance in ECFP space determines a low similarity between these two molecules given their disparate chemical structures, but have the complex molecular characteristics shared by these molecules been learned by **IGNITE**?

To rigorously answer this question, we randomly sample 100,000 small molecules and order all 100,002 small molecules (the 100,000 randomly sampled molecules + CHEMBL200234 and levisoprenaline) with respect to distance from CHEMBL200234 as well as levisoprenaline. We then extract and average the index of levisoprenaline in the ranked list of CHEMBL200234 and the index of CHEMBL200234 in the ranked list of levisoprenaline to determine a combined score.

Under Tanimoto distance, CHEMBL200234 places levisoprenaline at position 50,204 while levisoprenaline places CHEMBL200234 at position 67,119. In contrast, under the **IGNITE** embeddings distance, CHEMBL200234 places levisoprenaline at position 31,650 while levisoprenaline places CHEMBL200234 at position 34,551. This example—visualized in Figure 2—illustrates that molecules even with dissimilar chemical structures may be placed relatively close to one another in the **IGNITE** embedding space. Taken alongside Section 4.1, this finding lends support the hypothesis that molecular embeddings learned by pre-training on binding energies implicitly encode complex molecular characteristics.

## 5 Experiments and Discussion

Our aim is to determine if **IGNITE** improves few-shot learning performance on molecular property prediction. We build our analysis on two conditions reflecting the constraints often imposed on academia and industry where existing models are likely to run efficiently but a capacity — both human and computational — to implement new methods and tune them is limited:

- **Model Agnostic:** **IGNITE** should be applicable and effective across a diverse range of architectures and learning algorithms.

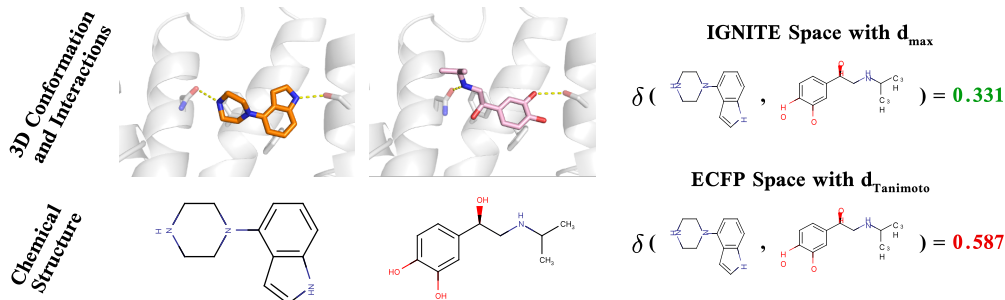


Figure 2: While these two molecules have very different 2D structures, they can adopt similar 3D conformations and form similar interactions with a target protein. Shown are renderings of these molecules in complex with the  $\beta_1$ -adrenergic receptor, with dashed yellow lines indicating hydrogen bonds. These molecules are relatively close in the embedding space, falling in the 33rd percentile amongst a randomly selected set of molecules, as compared to the 58th percentile using the Tanimoto coefficient in ECFP space.

- **Minimal Modification:** replacing the initial feature space with the **IGNITE** embedding space should be effective with minimal modification or hyperparameter tuning.

For our experimental evaluation, we choose FS-Mol [31], a few-shot learning benchmark designed to reflect the size and scope of datasets used in drug discovery, as well as 3 datasets from the MoleculeNet [38] benchmark suite.

**FS-Mol Description.** FS-Mol is a few-shot molecular property prediction benchmark that measures how small molecules interact with protein targets. The dataset spans 5,120 proteins and encompasses 233,786 different small molecules. On average, each protein has 94 small molecule measurements, and the benchmark is formulated to predict if one of these small molecules will inhibit (or not) the protein target.

The benchmark uses a unique metric,  $\Delta$ AUPRC, or the relative change in the area under the precision-recall curve (AUPRC) from a random guess baseline. The label distributions of many protein targets in FS-Mol are highly imbalanced; most small molecules will not inhibit a specific protein target. In this setting, measuring the relative change in AUPRC is often more informative than the absolute AUPRC so that targets with balanced labels do not marginalize performance improvements (or deteriorations) of targets with highly imbalanced labels.

**FS-Mol Experimental Setup.** Stanley et al. [31] presents several few-shot learning baselines for this benchmark. We select three of the best: multi-task pre-training with single-task fine-tuning (MT) [7], model-agnostic meta-learning (MAML) [13], and prototypical networks (PROTO) [30]. Our aim is to determine if their performance can be improved by simply modifying the molecular features on which they operate.

This selection of baselines fulfills our “Model Agnostic” criterion as the learning paradigms for MT, MAML, and PROTO are dissimilar. For instance, MT builds molecular representations amenable to all tasks, MAML learns representations that can be quickly adapted, and PROTO leverages a notion of distance—rather than inner product—in its learned representations to predict the label of a molecule. While each baseline is dissimilar, they all use a linear transformation to convert the input feature space to the model’s hidden dimension representation space. We simply replace this first hidden dimension representation space with the **IGNITE** embedding space. This change actually simplifies the few-shot learning algorithm, decreasing computational and runtime complexity, by removing the initial embedding layer.

Adhering to the “Minimum Modification” criterion, we do not perform any additional hyperparameter tuning for few-shot learning approaches using **IGNITE** embeddings. We simply use the hyperparameters found by Stanley et al. [31] for each baseline model. We prefix few-shot learning methods with an **IGNITE-** to indicate this model uses **IGNITE** embeddings.

**FS-Mol Results.** Table 2 indicates that **IGNITE** embeddings significantly improve MT performance on target inhibition prediction, and performance is most improved at smaller support size splits. This result is likely caused from **IGNITE** encoding complex molecular characteristics relevant for protein targets in the test set, characteristics that MT struggles to incorporate into its learned representations

Table 2: FS-Mol classification performance across the 157 targets in the FS-Mol test split. We report mean  $\Delta$ AUPRC and standard error from 10 training runs with different random seeds. Performance of MT, and MAML cited from [31]. PROTO is re-evaluated to use only graph-level features.

Method	Support Size				
	16	32	64	128	256
MT	0.112 $\pm$ 0.005	0.144 $\pm$ 0.006	0.177 $\pm$ 0.008	0.223 $\pm$ 0.008	0.237 $\pm$ 0.018
IGNITE-MT	0.157 $\pm$ 0.007	0.191 $\pm$ 0.008	0.221 $\pm$ 0.008	0.259 $\pm$ 0.009	0.281 $\pm$ 0.020
% change	$\Delta$ 40.2%	$\Delta$ 32.6%	$\Delta$ 24.9%	$\Delta$ 16.1%	$\Delta$ 18.6%
MAML	0.160 $\pm$ 0.008	0.167 $\pm$ 0.008	0.173 $\pm$ 0.008	0.192 $\pm$ 0.009	0.186 $\pm$ 0.019
IGNITE-MAML	0.164 $\pm$ 0.008	0.173 $\pm$ 0.008	0.183 $\pm$ 0.008	0.204 $\pm$ 0.008	0.193 $\pm$ 0.018
% change	$\Delta$ 2.5%	$\Delta$ 3.6%	$\Delta$ 5.8%	$\Delta$ 6.3%	$\Delta$ 3.8%
PROTO	0.185 $\pm$ 0.008	0.224 $\pm$ 0.009	0.256 $\pm$ 0.009	0.290 $\pm$ 0.009	0.263 $\pm$ 0.018
IGNITE-PROTO	0.195 $\pm$ 0.008	0.232 $\pm$ 0.009	0.263 $\pm$ 0.009	0.297 $\pm$ 0.009	0.283 $\pm$ 0.019
% change	$\Delta$ 5.4%	$\Delta$ 3.6%	$\Delta$ 2.7%	$\Delta$ 2.4%	$\Delta$ 7.6%

Table 3: Results on the BACE Classification dataset from the MoleculeNet benchmark suite. We report mean AUPRC as well as standard error averaged across 10 training runs with different random seeds.

Method	Support Size				
	16	32	64	128	256
MT	0.547 $\pm$ 0.064	0.600 $\pm$ 0.063	0.652 $\pm$ 0.051	0.696 $\pm$ 0.037	0.738 $\pm$ 0.028
IGNITE-MT	0.574 $\pm$ 0.08	0.674 $\pm$ 0.039	0.719 $\pm$ 0.025	0.739 $\pm$ 0.037	0.784 $\pm$ 0.014
% change	$\Delta$ 4.9%	$\Delta$ 12.3%	$\Delta$ 10.3%	$\Delta$ 6.2%	$\Delta$ 6.2%
MAML	0.510 $\pm$ 0.026	0.508 $\pm$ 0.035	0.548 $\pm$ 0.065	0.568 $\pm$ 0.075	0.649 $\pm$ 0.016
IGNITE-MAML	0.620 $\pm$ 0.027	0.633 $\pm$ 0.031	0.643 $\pm$ 0.043	0.668 $\pm$ 0.037	0.685 $\pm$ 0.041
% change	$\Delta$ 21.6%	$\Delta$ 24.6%	$\Delta$ 17.3%	$\Delta$ 17.6%	$\Delta$ 5.5%

from only 16 training examples. While the increase in performance declines as the support size increases, it ticks up at 256. This effect is similarly noted by Stanley et al. [31] and is caused by few protein targets in the test set actually containing at least 256 examples to evaluate the 256-size support split.

We also analyze if **IGNITE**—an approach developed with a multi-task learning paradigm—might also improve the performance of other few-shot learning algorithms like Prototypical Networks or MAML. This is a difficult proposition as the inductive biases fundamental to each learning algorithm are highly dissimilar. To our surprise, our findings in Table 2 show consistent improvement of PROTO and MAML across all support splits. It may be possible to achieve even larger performance improvements on PROTO and MAML by learning **IGNITE** embeddings with an approach that mirrors the down-stream few-shot learning algorithm. We leave this exploration to future work.

**MoleculeNet Description & Setup.** MoleculeNet [38] is a benchmark suite spanning many disparate molecular properties. While each dataset can stand alone, we adapt it to the few-shot learning setting by meta-training on the larger FS-Mol benchmark, sampling a support set from the MoleculeNet dataset, and designating all other examples in this dataset as the query set. As FS-Mol is a binary prediction benchmark, we limit ourselves to binary prediction tasks from the MoleculeNet benchmark and select BACE, HIV, and TOX21 for our experimental analysis.

BACE measures if a small molecule inhibits (or not) the human  $\beta$ -secretase-1 enzyme. It contains a single task and measurements for 1,522 small molecules. Tox21 measures the toxicity of small molecules for several different biological targets such as nuclear receptors and stress pathways. We filter out the targets with high class imbalance, and the resulting dataset contains 7,831 measures of toxicity across 4 targets. HIV measures if a small molecule will inhibit HIV replication. It is composed of a single task and spans 41,127 small molecules. This dataset is extremely unbalanced, and as both MT and MAML require at least two points from each class to be present—one for training and the other for early stopping when fine-tuning on the support set—we are unable to evaluate HIV at smaller support sizes.

As models are pre-trained on FS-Mol, we use the same fine-tuning hyperparameters and approach as in our earlier evaluation; no additional hyperparameter tuning is performed for **IGNITE**. However dissimilar to our analysis on FS-Mol, we report AUPRC, or the area under the precision-recall curve,

Table 4: Tox21 classification performance across 4 targets that measure the toxicity of a small molecule with a certain biological pathway or nuclear receptor. We report mean AUPRC as well as standard error averaged across 10 training runs with different random seeds.

Method	Support Size				
	16	32	64	128	256
MT	0.120 ± 0.006	0.140 ± 0.013	0.155 ± 0.015	0.166 ± 0.019	0.198 ± 0.025
IGNITE-MT	0.150 ± 0.017	0.148 ± 0.017	0.173 ± 0.019	0.194 ± 0.031	0.242 ± 0.034
% change	<b>Δ25.1%</b>	<b>Δ5.9%</b>	<b>Δ11.7%</b>	<b>Δ16.6%</b>	<b>Δ22.8%</b>
MAML	0.131 ± 0.009	0.130 ± 0.009	0.131 ± 0.009	0.131 ± 0.010	0.134 ± 0.008
IGNITE-MAML	0.124 ± 0.009	0.134 ± 0.010	0.136 ± 0.011	0.142 ± 0.012	0.163 ± 0.020
% change	<b>-Δ5.2%</b>	<b>Δ3.1%</b>	<b>Δ3.8%</b>	<b>Δ8.2%</b>	<b>Δ21.7%</b>

to align our evaluation with the MoleculeNet benchmark [38]. Moreover, due to implementation challenges, we drop our evaluation of PROTO to focus on MT and MAML.

**MoleculeNet Results.** Our results on MoleculeNet datasets reflect our findings on FS-Mol: **IGNITE** appears to almost universally improve few-shot learning performance. Starting with the BACE Classification dataset measuring inhibition of the  $\beta$ -secretase-1 enzyme, we find augmenting MT and MAML with **IGNITE** embeddings substantively improves performance across all support sizes. Our findings are summarized in Table 3. However, unlike our findings on FS-Mol, this time MAML benefits the most, improving AUPRC by almost 25% at 32 support size.

Similar results manifest for the Tox 21 evaluation measuring small molecule toxicities. As shown in Table 4, the performance of MT and MAML is improved across all support splits except at the 16 support size for MAML. As performance is degraded for the smallest support size, and given the performance improvements at all other support splits, we posit this result may be an outlier caused by an especially detrimental random seed when sampling support-set points for fine-tuning. Smaller support splits are more sensitive to sampling, where the choice of training examples has an outsized influence on model predictions.

The HIV benchmark, measuring if a small molecule inhibits HIV replication, further supports our prior findings that **IGNITE** substantively increases AUPRC for both MT and MAML as shown in Table 5. This dataset is especially challenging given its extreme label imbalance. As MT and MAML require at least two points from each class in the support set, we are unable to evaluate this dataset at smaller support splits. However, this setup actually closely mirrors real-life drug discovery where exceedingly few molecules manifest a desired property. It is particularly exciting that **IGNITE** appears to improve the performance of few-shot learning methods on these types of data distributions.

## 6 Conclusion

In this work, we develop molecular embeddings that encode complex molecular characteristics—such as the various 3D geometries a molecule may adopt or the types of chemical interactions it can form—to improve the performance of few-shot learning algorithms on molecular property prediction. Our analysis of the **IGNITE** embedding space suggests these characteristics are in fact encoded by the embeddings. Further, our empirical analysis on 4 molecular property prediction benchmarks, with properties ranging from the inhibition of protein targets to the toxicity of small molecules, suggests **IGNITE** almost universally improves the performance of 3 popular, but very different, few-shot learning algorithms. Moreover, integrating **IGNITE** into few-shot learning algorithms takes minimum modification and does not require additional hyperparameter tuning.

It is our hope that future work will improve upon our approach. Possible avenues for improvement may include leveraging recent advances in generative diffusion models to replace physics-based molecular docking or scaling up to even more synthetic data and expressive architectures.

Table 5: Results on the HIV dataset from the MoleculeNet benchmark suite. We report mean AUPRC as well as standard error averaged across 10 training runs with different random seeds.

Method	Support Size	
	128	256
MT	0.062 ± 0.035	0.078 ± 0.033
IGNITE-MT	0.066 ± 0.029	0.087 ± 0.035
% change	<b>Δ6.5%</b>	<b>Δ11.5%</b>
MAML	0.053 ± 0.015	0.060 ± 0.023
IGNITE-MAML	0.070 ± 0.021	0.068 ± 0.016
% change	<b>Δ32.1%</b>	<b>Δ13.3%</b>

## Acknowledgments and Disclosure of Funding

We gratefully acknowledge the support of DARPA under Nos. HR00112190039 (TAMI), N660011924033 (MCS); ARO under Nos. W911NF-16-1-0342 (MURI), W911NF-16-1-0171 (DURIP); NSF under Nos. OAC-1835598 (CINES), OAC-1934578 (HDR), CCF-1918940 (Expeditions), NIH under No. 3U54HG010426-04S1 (HuBMAP), Stanford Data Science Initiative, Wu Tsai Neurosciences Institute, Amazon, Docomo, GSK, Hitachi, Intel, JPMorgan Chase, Juniper Networks, KDDI, NEC, and Toshiba.

The content is solely the responsibility of the authors and does not necessarily represent the official views of the funding entities.

## References

- [1] Walid Ahmad, Elana Simon, Seyone Chithrananda, Gabriel Grand, and Bharath Ramsundar. Chemberta-2: Towards chemical foundation models. *arXiv preprint arXiv:2209.01712*, 2022.
- [2] Han Altae-Tran, Bharath Ramsundar, Aneesh S Pappu, and Vijay Pande. Low data drug discovery with one-shot learning. *ACS central science*, 3(4), 2017.
- [3] Antreas Antoniou, Harri Edwards, and Amos Storkey. How to train your maml. In *Seventh International Conference on Learning Representations*, 2019.
- [4] Thomas Bachlechner, Bodhisattwa Prasad Majumder, Henry Mao, Gary Cottrell, and Julian McAuley. Rezero is all you need: Fast convergence at large depth. In *Uncertainty in Artificial Intelligence*. PMLR, 2021.
- [5] Caterina Bissantz, Bernd Kuhn, and Martin Stahl. A medicinal chemist’s guide to molecular interactions. *Journal of medicinal chemistry*, 53(14), 2010.
- [6] David C Blakemore, Luis Castro, Ian Churcher, David C Rees, Andrew W Thomas, David M Wilson, and Anthony Wood. Organic synthesis provides opportunities to transform drug discovery. *Nature chemistry*, 10(4), 2018.
- [7] Rich Caruana. Multitask learning. *Machine learning*, 28(1), 1997.
- [8] Wenlin Chen, Austin Tripp, and José Miguel Hernández-Lobato. Meta-learning feature representations for adaptive gaussian processes via implicit differentiation. *arXiv preprint arXiv:2205.02708*, 2022.
- [9] Kangway V Chuang, Laura M Gunsalus, and Michael J Keiser. Learning molecular representations for medicinal chemistry: miniperspective. *Journal of Medicinal Chemistry*, 63(16), 2020.
- [10] Gabriele Corso, Luca Cavalleri, Dominique Beaini, Pietro Liò, and Petar Veličković. Principal neighbourhood aggregation for graph nets. *Advances in Neural Information Processing Systems*, 33, 2020.
- [11] Xiaomin Fang, Lihang Liu, Jieqiong Lei, Donglong He, Shanzhuo Zhang, Jingbo Zhou, Fan Wang, Hua Wu, and Haifeng Wang. Chemrl-gem: Geometry enhanced molecular representation learning for property prediction. *arXiv preprint arXiv:2106.06130*, 2021.
- [12] Evan N Feinberg, Elizabeth Joshi, Vijay S Pande, and Alan C Cheng. Improvement in admet prediction with multitask deep featurization. *Journal of medicinal chemistry*, 63(16), 2020.
- [13] Chelsea Finn, Pieter Abbeel, and Sergey Levine. Model-agnostic meta-learning for fast adaptation of deep networks. In *International conference on machine learning*. PMLR, 2017.
- [14] Richard A Friesner, Jay L Banks, Robert B Murphy, Thomas A Halgren, Jasna J Klicic, Daniel T Mainz, Matthew P Repasky, Eric H Knoll, Mee Shelley, Jason K Perry, et al. Glide: a new approach for rapid, accurate docking and scoring. 1. method and assessment of docking accuracy. *Journal of medicinal chemistry*, 47(7), 2004.

- [15] Justin Gilmer, Samuel S Schoenholz, Patrick F Riley, Oriol Vinyals, and George E Dahl. Neural message passing for quantum chemistry. In *International conference on machine learning*. PMLR, 2017.
- [16] Kaveh Hassani and Amir Hosein Khasahmadi. Contrastive multi-view representation learning on graphs. In *International Conference on Machine Learning*. PMLR, 2020.
- [17] W Hu, B Liu, J Gomes, M Zitnik, P Liang, V Pande, and J Leskovec. Strategies for pre-training graph neural networks. In *International Conference on Learning Representations (ICLR)*, 2020.
- [18] Matthew P. Jacobson, Richard A. Friesner, Zhexin Xiang, and Barry Honig. On the role of the crystal environment in determining protein side-chain conformations. *Journal of Molecular Biology*, 320(3), 2002. ISSN 0022-2836. doi: 10.1016/S0022-2836(02)00470-9. URL <http://www.sciencedirect.com/science/article/pii/S0022283602004709>.
- [19] Rui Jiao, Jiaqi Han, Wenbing Huang, Yu Rong, and Yang Liu. Energy-motivated equivariant pretraining for 3d molecular graphs. In *Proceedings of the AAAI Conference on Artificial Intelligence*, volume 37, 2023.
- [20] Maurice G Kendall. *A Course in the Geometry of n Dimensions*. Courier Corporation, 2004.
- [21] DP Kingma. Adam: a method for stochastic optimization. In *Int Conf Learn Represent*, 2014.
- [22] Olga Maria Lage, María C Ramos, Rita Calisto, Eduarda Almeida, Vitor Vasconcelos, and Francisca Vicente. Current screening methodologies in drug discovery for selected human diseases. *Marine drugs*, 16(8), 2018.
- [23] Shuangli Li, Jingbo Zhou, Tong Xu, Dejing Dou, and Hui Xiong. Geomgcl: Geometric graph contrastive learning for molecular property prediction. In *Proceedings of the AAAI Conference on Artificial Intelligence*, volume 36, 2022.
- [24] Łukasz Maziarka, Tomasz Danel, Sławomir Mucha, Krzysztof Rataj, Jacek Tabor, and Stanisław Jastrzębski. Molecule attention transformer. *arXiv preprint arXiv:2002.08264*, 2020.
- [25] Stephen Merity. Single headed attention rnn: Stop thinking with your head. *arXiv preprint arXiv:1911.11423*, 2019.
- [26] S Parasuraman. Toxicological screening. *Journal of pharmacology & pharmacotherapeutics*, 2(2), 2011.
- [27] David Rogers and Mathew Hahn. Extended-connectivity fingerprints. *Journal of chemical information and modeling*, 50(5), 2010.
- [28] Yu Rong, Yatao Bian, Tingyang Xu, Weiyang Xie, Ying Wei, Wenbing Huang, and Junzhou Huang. Self-supervised graph transformer on large-scale molecular data. *Advances in Neural Information Processing Systems*, 33, 2020.
- [29] Johannes Schimunek, Philipp Seidl, Lukas Friedrich, Daniel Kuhn, Friedrich Rippmann, Sepp Hochreiter, and Günter Klambauer. Context-enriched molecule representations improve few-shot drug discovery. In *The Eleventh International Conference on Learning Representations*, 2022.
- [30] Jake Snell, Kevin Swersky, and Richard Zemel. Prototypical networks for few-shot learning. *Advances in neural information processing systems*, 30, 2017.
- [31] Megan Stanley, John F Bronskill, Krzysztof Maziarz, Hubert Misztela, Jessica Lanini, Marwin Segler, Nadine Schneider, and Marc Brockschmidt. Fs-mol: A few-shot learning dataset of molecules. In *Thirty-fifth Conference on Neural Information Processing Systems Datasets and Benchmarks Track (Round 2)*, 2021.
- [32] Ruoxi Sun, Hanjun Dai, and Adams Wei Yu. Does gnn pretraining help molecular representation? *Advances in Neural Information Processing Systems*, 35, 2022.

- [33] Hugo Touvron, Matthieu Cord, Alexandre Sablayrolles, Gabriel Synnaeve, and Hervé Jégou. Going deeper with image transformers. In *Proceedings of the IEEE/CVF International Conference on Computer Vision*, 2021.
- [34] Ashish Vaswani, Noam Shazeer, Niki Parmar, Jakob Uszkoreit, Llion Jones, Aidan N Gomez, Łukasz Kaiser, and Illia Polosukhin. Attention is all you need. *Advances in neural information processing systems*, 30, 2017.
- [35] Yaqing Wang, Abulikemu Abuduweili, Quanming Yao, and Dejing Dou. Property-aware relation networks for few-shot molecular property prediction. *Advances in Neural Information Processing Systems*, 34, 2021.
- [36] Michael J Waring, John Arrowsmith, Andrew R Leach, Paul D Leeson, Sam Mandrell, Robert M Owen, Garry Pairaudeau, William D Pennie, Stephen D Pickett, Jibo Wang, et al. An analysis of the attrition of drug candidates from four major pharmaceutical companies. *Nature reviews Drug discovery*, 14(7), 2015.
- [37] Lirong Wu, Haitao Lin, Cheng Tan, Zhangyang Gao, and Stan Z Li. Self-supervised learning on graphs: Contrastive, generative, or predictive. *IEEE Transactions on Knowledge and Data Engineering*, 2021.
- [38] Zhenqin Wu, Bharath Ramsundar, Evan N Feinberg, Joseph Gomes, Caleb Geniesse, Aneesh S Pappu, Karl Leswing, and Vijay Pande. Moleculenet: a benchmark for molecular machine learning. *Chemical science*, 9(2), 2018.
- [39] Ruibin Xiong, Yunchang Yang, Di He, Kai Zheng, Shuxin Zheng, Chen Xing, Huishuai Zhang, Yanyan Lan, Liwei Wang, and Tieyan Liu. On layer normalization in the transformer architecture. In *International Conference on Machine Learning*. PMLR, 2020.
- [40] Kevin Yang, Kyle Swanson, Wengong Jin, Connor Coley, Philipp Eiden, Hua Gao, Angel Guzman-Perez, Timothy Hopper, Brian Kelley, Miriam Mathea, et al. Analyzing learned molecular representations for property prediction. *Journal of chemical information and modeling*, 59(8), 2019.
- [41] Yuning You, Tianlong Chen, Yongduo Sui, Ting Chen, Zhangyang Wang, and Yang Shen. Graph contrastive learning with augmentations. *Advances in Neural Information Processing Systems*, 33, 2020.
- [42] Sheheryar Zaidi, Michael Schaarschmidt, James Martens, Hyunjik Kim, Yee Whye Teh, Alvaro Sanchez-Gonzalez, Peter Battaglia, Razvan Pascanu, and Jonathan Godwin. Pre-training via denoising for molecular property prediction. *arXiv preprint arXiv:2206.00133*, 2022.
- [43] Yanqiao Zhu, Yichen Xu, Feng Yu, Qiang Liu, Shu Wu, and Liang Wang. Graph contrastive learning with adaptive augmentation. In *Proceedings of the Web Conference 2021*, 2021.

## Appendix

### A GLIDE Protocol

To produce synthetic data, we used the physics-based docking method GLIDE [14] (Schrödinger Release 2022-2: Maestro, Schrödinger, LLC, New York, NY, 2022). Running GLIDE can be separated into three steps: preparation of small molecules, preparation of protein structures, and the docking of the prepared small molecules into the prepared protein structures.

To prepare a set of small molecules to be docked, we began with a selection of 32,547 small molecules from ChEMBL. Importantly, we used ChEMBL simply to provide examples of small molecules; we took the SMILES strings and did not use the annotated activities in any way. We then used the Schrodinger ligprep tool to enumerate relevant tautomeric states (e.g. protonation states) and, if not specified in the SMILES strings, up to 32 stereoisomers.

To prepare a set of protein structures, we began with a set of 1,601 structures from the PDBBind database. Schrodinger prepwizard was used to add hydrogens, choose tautomeric states, and perform a constrained minimization (heavy atoms within 0.3 Å of starting coordinates) using default parameters [18]. The small molecule annotated in PDBBind was used to center the docking site, but was otherwise not used in any way.

Docking was run using GLIDE in SP mode using default parameters. The docking score for a given small molecule–protein pair was defined as the most favorable score encountered for any tautomeric state of the small molecule, taking into account penalties for choosing an unfavorable tautomeric state. Due to this, it might be that IGNITE encodes an implicit representation of a molecule’s potential tautomeric states in addition to potential 3D geometries and chemical interactions. Docking calculations were attempted for all small molecule–protein pairs but in some cases docking failed to produce any reasonable poses or the job failed for other reasons so these pairs weren’t considered.

### B Experimental Design

We offer additional details related to the training of IGNITE . While this description can be valuable to some readers, we direct those interested in reproducing our findings or building on our framework to access the code directly. Our code is released in the supplementary material download on OpenReview; however, due to the synthetic data occupying 77 GB on disk, we are unable to upload (or link to) the dataset without breaking anonymity.

#### B.1 Additional Training Details

Our architecture employs a learning rate of  $5e-5$  for the shared parameters and a learning rate of  $1e-4$  for the task-specific parameters. We use a linear warm-up scheduler for 100 steps (starting at 0 and ending at the specified learning rate) for both shared and task-specific learning rates. The training process also leverages Adam [21] with default Pytorch parameters and uses a batch size of 256 molecules. With regards to the task-specific parameters in the IGNITE multi-task

training paradigm, the output from the graph readout is passed through a shared MLP of hidden dimension 512 and then uses a task-specific projection layer of dimension  $[512 \times 1]$  for each target. Table 6 offers a comparison of the total number of small molecules as well as the number of tasks in each benchmark that we use for evaluation. For our experiments, we used a single 80 GB Nvidia A100 GPU, with the model taking approximately 10 GB of memory on the GPU.

Table 6: Benchmark comparison.

Dataset	# tasks	# compounds
FS-Mol Test	157	27520
BACE	1	1522
Tox21	4	7831
HIV	1	41127

### C Additional FS-Mol Experimental Results

To offer additional insight into the FS-Mol empirical findings in section 5, we present a per-target breakdown of the first 50 targets in the test set of FS-Mol across support size splits of 16, 32, 64, 128,

and 256. Table 7 depicts these results for the Multi-Task Learning baseline, Table 8 depicts these results for the Prototypical Networks baseline, and Table 9 depicts these results from the MAML baseline. Highlighted values indicate the highest result for this target at the given support size.

Table 7: Multi-Task Results measuring  $\Delta$ AUPRC on the first 50 tasks in the test set of FS-Mol.

TASK-ID	16 (IGNITE-MT)	32 (IGNITE-MT)	64 (IGNITE-MT)	128 (IGNITE-MT)	256 (IGNITE)	16 (MT)	32 (MT)	64 (MT)	128 (MT)	256 (MT)
1006005	0.57 ± 0.05	0.62 ± 0.04	0.63 ± 0.05	0.62 ± 0.05	nan	0.54 ± 0.03	0.54 ± 0.03	0.55 ± 0.03	0.56 ± 0.06	nan
1066254	0.71 ± 0.07	0.73 ± 0.06	0.81 ± 0.06	0.83 ± 0.10	nan	0.65 ± 0.05	0.64 ± 0.09	0.77 ± 0.07	0.86 ± 0.11	nan
1119333	0.69 ± 0.08	0.73 ± 0.05	0.78 ± 0.03	0.82 ± 0.03	0.85 ± 0.02	0.69 ± 0.07	0.72 ± 0.05	0.76 ± 0.02	0.79 ± 0.04	0.84 ± 0.04
1243967	0.62 ± 0.08	0.72 ± 0.09	0.74 ± 0.05	0.80 ± 0.05	nan	0.63 ± 0.07	0.66 ± 0.05	0.71 ± 0.04	0.76 ± 0.05	nan
1243970	0.66 ± 0.06	0.70 ± 0.04	0.75 ± 0.05	0.77 ± 0.04	nan	0.63 ± 0.06	0.65 ± 0.04	0.70 ± 0.02	0.75 ± 0.05	nan
1613777	0.52 ± 0.03	0.53 ± 0.04	0.55 ± 0.02	0.57 ± 0.03	0.59 ± 0.02	0.52 ± 0.04	0.53 ± 0.02	0.54 ± 0.02	0.57 ± 0.02	0.59 ± 0.02
1613800	0.42 ± 0.02	0.45 ± 0.03	0.49 ± 0.02	0.45 ± 0.02	0.47 ± 0.02	0.42 ± 0.03	0.42 ± 0.01	0.43 ± 0.02	0.45 ± 0.02	0.47 ± 0.01
1613898	0.53 ± 0.03	0.54 ± 0.06	0.56 ± 0.04	0.60 ± 0.07	nan	0.55 ± 0.04	0.54 ± 0.06	0.58 ± 0.04	0.61 ± 0.08	nan
1613907	0.62 ± 0.06	0.62 ± 0.08	0.63 ± 0.08	0.66 ± 0.14	nan	0.60 ± 0.05	0.62 ± 0.07	0.67 ± 0.06	0.70 ± 0.15	nan
1613926	0.67 ± 0.07	0.69 ± 0.06	0.74 ± 0.06	0.85 ± 0.14	nan	0.61 ± 0.04	0.60 ± 0.06	0.69 ± 0.06	0.73 ± 0.19	nan
1613949	0.47 ± 0.08	0.46 ± 0.06	0.54 ± 0.04	0.62 ± 0.12	nan	0.45 ± 0.06	0.45 ± 0.06	0.52 ± 0.06	0.56 ± 0.12	nan
1614027	0.54 ± 0.03	0.56 ± 0.04	0.60 ± 0.03	0.66 ± 0.02	0.69 ± 0.03	0.53 ± 0.03	0.56 ± 0.04	0.59 ± 0.03	0.63 ± 0.02	0.66 ± 0.02
1614153	0.36 ± 0.01	0.38 ± 0.03	0.38 ± 0.03	0.40 ± 0.02	0.40 ± 0.02	0.36 ± 0.02	0.37 ± 0.03	0.37 ± 0.02	0.38 ± 0.03	0.39 ± 0.01
1614292	0.37 ± 0.03	0.37 ± 0.02	0.38 ± 0.02	0.38 ± 0.02	0.39 ± 0.01	0.36 ± 0.02	0.37 ± 0.01	0.38 ± 0.02	0.38 ± 0.01	0.38 ± 0.02
1614423	0.66 ± 0.12	0.68 ± 0.10	0.72 ± 0.05	0.77 ± 0.04	0.82 ± 0.02	0.52 ± 0.05	0.54 ± 0.05	0.59 ± 0.05	0.67 ± 0.04	0.74 ± 0.04
1614433	0.45 ± 0.04	0.47 ± 0.06	0.48 ± 0.04	0.50 ± 0.02	0.55 ± 0.04	0.45 ± 0.04	0.47 ± 0.05	0.47 ± 0.04	0.49 ± 0.03	0.53 ± 0.04
1614466	0.47 ± 0.04	0.48 ± 0.05	0.49 ± 0.03	0.49 ± 0.05	0.50 ± 0.03	0.46 ± 0.05	0.47 ± 0.05	0.47 ± 0.04	0.48 ± 0.04	0.48 ± 0.02
1614503	0.47 ± 0.08	0.48 ± 0.09	0.52 ± 0.05	0.73 ± 0.21	nan	0.44 ± 0.05	0.44 ± 0.06	0.48 ± 0.08	0.66 ± 0.22	nan
1614508	0.74 ± 0.10	0.85 ± 0.02	0.87 ± 0.02	0.90 ± 0.04	nan	0.76 ± 0.07	0.85 ± 0.04	0.87 ± 0.03	0.91 ± 0.05	nan
1614522	0.58 ± 0.04	0.61 ± 0.04	0.62 ± 0.03	0.66 ± 0.01	0.66 ± 0.03	0.54 ± 0.04	0.55 ± 0.02	0.56 ± 0.02	0.58 ± 0.03	0.60 ± 0.02
1737951	0.64 ± 0.10	0.67 ± 0.06	0.79 ± 0.05	0.85 ± 0.08	nan	0.55 ± 0.06	0.60 ± 0.08	0.63 ± 0.05	0.72 ± 0.07	nan
1738079	0.50 ± 0.02	0.50 ± 0.04	0.49 ± 0.03	0.48 ± 0.03	nan	0.52 ± 0.04	0.52 ± 0.04	0.53 ± 0.03	0.56 ± 0.05	nan
1738362	0.51 ± 0.10	0.46 ± 0.08	0.59 ± 0.09	0.75 ± 0.20	nan	0.52 ± 0.07	0.56 ± 0.11	0.62 ± 0.05	0.84 ± 0.14	nan
1738395	0.51 ± 0.04	0.49 ± 0.05	0.59 ± 0.04	0.54 ± 0.04	nan	0.49 ± 0.04	0.48 ± 0.03	0.50 ± 0.05	0.51 ± 0.05	nan
1738485	0.56 ± 0.02	0.55 ± 0.03	0.58 ± 0.06	0.59 ± 0.04	0.65 ± 0.06	0.54 ± 0.04	0.56 ± 0.03	0.58 ± 0.04	0.60 ± 0.06	0.68 ± 0.06
1738502	0.47 ± 0.06	0.50 ± 0.06	0.53 ± 0.05	0.53 ± 0.03	0.58 ± 0.03	0.37 ± 0.03	0.39 ± 0.02	0.42 ± 0.03	0.45 ± 0.02	0.49 ± 0.04
1738573	0.51 ± 0.02	0.52 ± 0.03	0.54 ± 0.03	0.55 ± 0.02	0.57 ± 0.01	0.52 ± 0.02	0.53 ± 0.01	0.53 ± 0.01	0.54 ± 0.01	0.56 ± 0.02
1738579	0.58 ± 0.05	0.59 ± 0.05	0.59 ± 0.04	0.67 ± 0.04	nan	0.52 ± 0.03	0.54 ± 0.04	0.56 ± 0.03	0.62 ± 0.04	nan
1738633	0.59 ± 0.06	0.68 ± 0.04	0.71 ± 0.06	0.70 ± 0.08	nan	0.57 ± 0.05	0.60 ± 0.08	0.60 ± 0.05	0.71 ± 0.10	nan
1794324	0.52 ± 0.04	0.54 ± 0.03	0.55 ± 0.03	0.57 ± 0.01	0.60 ± 0.01	0.53 ± 0.03	0.54 ± 0.03	0.56 ± 0.03	0.58 ± 0.02	0.60 ± 0.02
1794504	0.72 ± 0.06	0.75 ± 0.05	0.81 ± 0.04	0.85 ± 0.24	nan	0.67 ± 0.04	0.67 ± 0.06	0.73 ± 0.05	0.90 ± 0.21	nan
1794519	0.69 ± 0.08	0.73 ± 0.05	0.79 ± 0.02	0.81 ± 0.05	nan	0.70 ± 0.06	0.72 ± 0.05	0.80 ± 0.03	0.77 ± 0.07	nan
1794557	0.52 ± 0.04	0.53 ± 0.03	0.56 ± 0.04	0.58 ± 0.04	0.60 ± 0.02	0.51 ± 0.03	0.53 ± 0.02	0.53 ± 0.03	0.53 ± 0.01	0.54 ± 0.03
1963701	0.54 ± 0.03	0.54 ± 0.02	0.58 ± 0.04	0.61 ± 0.04	0.65 ± 0.03	0.53 ± 0.03	0.54 ± 0.04	0.56 ± 0.03	0.58 ± 0.03	0.63 ± 0.03
1963705	0.67 ± 0.09	0.75 ± 0.05	0.78 ± 0.03	0.82 ± 0.03	0.84 ± 0.02	0.65 ± 0.07	0.70 ± 0.06	0.73 ± 0.04	0.78 ± 0.03	0.82 ± 0.02
1963715	0.61 ± 0.05	0.59 ± 0.08	0.68 ± 0.04	0.72 ± 0.04	0.75 ± 0.02	0.50 ± 0.06	0.50 ± 0.06	0.56 ± 0.04	0.60 ± 0.03	0.65 ± 0.03
1963721	0.45 ± 0.08	0.48 ± 0.08	0.55 ± 0.06	0.57 ± 0.07	0.71 ± 0.09	0.38 ± 0.05	0.42 ± 0.04	0.44 ± 0.03	0.50 ± 0.05	0.61 ± 0.08
1963723	0.70 ± 0.10	0.75 ± 0.09	0.80 ± 0.03	0.84 ± 0.02	0.86 ± 0.02	0.61 ± 0.05	0.69 ± 0.05	0.74 ± 0.04	0.78 ± 0.03	0.81 ± 0.02
1963731	0.74 ± 0.06	0.79 ± 0.03	0.82 ± 0.02	0.87 ± 0.02	0.89 ± 0.02	0.63 ± 0.08	0.70 ± 0.04	0.75 ± 0.02	0.79 ± 0.03	0.82 ± 0.02
1963741	0.60 ± 0.05	0.79 ± 0.04	0.79 ± 0.03	0.75 ± 0.03	0.78 ± 0.02	0.51 ± 0.08	0.57 ± 0.06	0.59 ± 0.05	0.64 ± 0.04	0.71 ± 0.03
1963756	0.63 ± 0.09	0.75 ± 0.04	0.77 ± 0.02	0.80 ± 0.02	0.83 ± 0.02	0.57 ± 0.07	0.67 ± 0.05	0.69 ± 0.06	0.75 ± 0.02	0.79 ± 0.02
1963773	0.59 ± 0.06	0.61 ± 0.07	0.65 ± 0.04	0.69 ± 0.03	0.72 ± 0.02	0.54 ± 0.06	0.57 ± 0.06	0.61 ± 0.05	0.65 ± 0.03	0.70 ± 0.03
1963799	0.58 ± 0.07	0.64 ± 0.04	0.68 ± 0.04	0.71 ± 0.03	0.74 ± 0.04	0.48 ± 0.06	0.55 ± 0.05	0.58 ± 0.07	0.63 ± 0.05	0.68 ± 0.07
1963810	0.78 ± 0.06	0.81 ± 0.05	0.85 ± 0.02	0.86 ± 0.02	0.88 ± 0.01	0.67 ± 0.06	0.73 ± 0.05	0.76 ± 0.06	0.80 ± 0.04	0.84 ± 0.02
1963818	0.71 ± 0.05	0.74 ± 0.04	0.78 ± 0.03	0.80 ± 0.03	0.82 ± 0.02	0.66 ± 0.07	0.68 ± 0.06	0.72 ± 0.03	0.76 ± 0.03	0.79 ± 0.02
1963819	0.61 ± 0.07	0.67 ± 0.06	0.73 ± 0.06	0.77 ± 0.05	0.82 ± 0.01	0.48 ± 0.05	0.56 ± 0.07	0.60 ± 0.08	0.68 ± 0.06	0.77 ± 0.02
1963824	0.59 ± 0.05	0.66 ± 0.05	0.70 ± 0.03	0.74 ± 0.03	0.77 ± 0.05	0.54 ± 0.04	0.59 ± 0.05	0.64 ± 0.04	0.64 ± 0.04	0.69 ± 0.03
1963825	0.62 ± 0.06	0.69 ± 0.04	0.70 ± 0.05	0.75 ± 0.05	0.81 ± 0.04	0.57 ± 0.04	0.61 ± 0.04	0.64 ± 0.04	0.65 ± 0.04	0.69 ± 0.03
1963827	0.74 ± 0.09	0.78 ± 0.06	0.84 ± 0.03	0.86 ± 0.01	0.88 ± 0.02	0.71 ± 0.06	0.72 ± 0.08	0.79 ± 0.05	0.82 ± 0.02	0.84 ± 0.02
1963831	0.61 ± 0.10	0.69 ± 0.07	0.76 ± 0.02	0.78 ± 0.04	0.81 ± 0.05	0.55 ± 0.11	0.61 ± 0.07	0.69 ± 0.06	0.74 ± 0.05	0.77 ± 0.04
1963838	0.56 ± 0.04	0.57 ± 0.05	0.59 ± 0.06	0.67 ± 0.05	nan	0.54 ± 0.05	0.55 ± 0.04	0.58 ± 0.04	0.62 ± 0.06	nan

Table 8: PROTO Results measuring  $\Delta$ AUPRC on the first 50 tasks in the test set of FS-Mol.

TASK-ID	16 (IGNITE-PROTO)	32 (IGNITE-PROTO)	64 (IGNITE-PROTO)	128 (IGNITE-PROTO)	256 (IGNITE-PROTO)	16 (PROTO)	32 (PROTO)	64 (PROTO)	128 (PROTO)	256 (PROTO)
1006005	0.61 ± 0.05	0.63 ± 0.04	0.66 ± 0.04	0.69 ± 0.06	nan	0.56 ± 0.06	0.61 ± 0.05	0.65 ± 0.03	0.66 ± 0.07	nan
1066254	0.72 ± 0.07	0.77 ± 0.06	0.84 ± 0.04	0.87 ± 0.10	nan	0.71 ± 0.08	0.78 ± 0.06	0.82 ± 0.06	0.85 ± 0.08	nan
1119333	0.73 ± 0.05	0.74 ± 0.06	0.78 ± 0.03	0.82 ± 0.02	0.84 ± 0.04	0.71 ± 0.06	0.72 ± 0.04	0.78 ± 0.03	0.81 ± 0.02	0.83 ± 0.04
1243967	0.78 ± 0.03	0.81 ± 0.04	0.83 ± 0.03	0.84 ± 0.03	nan	0.73 ± 0.05	0.76 ± 0.04	0.80 ± 0.03	0.81 ± 0.03	nan
1243970	0.75 ± 0.03	0.79 ± 0.04	0.81 ± 0.03	0.85 ± 0.03	nan	0.71 ± 0.07	0.74 ± 0.04	0.81 ± 0.03	0.82 ± 0.03	nan
1613777	0.52 ± 0.02	0.54 ± 0.03	0.56 ± 0.03	0.59 ± 0.02	0.61 ± 0.02	0.52 ± 0.04	0.54 ± 0.04	0.57 ± 0.03	0.60 ± 0.04	0.62 ± 0.03
1613800	0.42 ± 0.02	0.44 ± 0.02	0.46 ± 0.02	0.48 ± 0.02	0.50 ± 0.01	0.41 ± 0.03	0.43 ± 0.03	0.45 ± 0.02	0.46 ± 0.02	0.48 ± 0.02
1613898	0.52 ± 0.02	0.55 ± 0.04	0.54 ± 0.04	0.61 ± 0.07	nan	0.55 ± 0.04	0.55 ± 0.05	0.55 ± 0.03	0.57 ± 0.08	nan
1613907	0.56 ± 0.04	0.58 ± 0.04	0.63 ± 0.04	0.64 ± 0.14	nan	0.55 ± 0.06	0.62 ± 0.06	0.66 ± 0.07	0.68 ± 0.10	nan
1613926	0.70 ± 0.04	0.74 ± 0.06	0.77 ± 0.04	0.88 ± 0.12	nan	0.65 ± 0.08	0.70 ± 0.06	0.76 ± 0.04	0.86 ± 0.15	nan
1613949	0.57 ± 0.08	0.65 ± 0.05	0.67 ± 0.06	0.67 ± 0.10	nan	0.51 ± 0.04	0.57 ± 0.04	0.58 ± 0.05	0.65 ± 0.11	nan
1614027	0.53 ± 0.02	0.57 ± 0.02	0.60 ± 0.03	0.64 ± 0.02	0.67 ± 0.02	0.55 ± 0.02	0.57 ± 0.01	0.61 ± 0.04	0.64 ± 0.02	0.67 ± 0.02
1614153	0.35 ± 0.02	0.37 ± 0.01	0.36 ± 0.02	0.39 ± 0.01	0.41 ± 0.01	0.34 ± 0.03	0.37 ± 0.02	0.37 ± 0.02	0.39 ± 0.01	0.41 ± 0.01
1614292	0.36 ± 0.02	0.38 ± 0.03	0.39 ± 0.02	0.40 ± 0.02	0.41 ± 0.02	0.36 ± 0.02	0.39 ± 0.02	0.41 ± 0.02	0.42 ± 0.03	0.44 ± 0.02
1614423	0.68 ± 0.06	0.72 ± 0.04	0.76 ± 0.02	0.78 ± 0.02	0.79 ± 0.04	0.54 ± 0.07	0.58 ± 0.05	0.67 ± 0.04	0.73 ± 0.02	0.77 ± 0.02
1614433	0.49 ± 0.04	0.50 ± 0.04	0.51 ± 0.03	0.53 ± 0.02	0.54 ± 0.02	0.46 ± 0.04	0.48 ± 0.02	0.48 ± 0.03	0.52 ± 0.03	0.54 ± 0.04
1614466	0.47 ± 0.03	0.48 ± 0.04	0.49 ± 0.01	0.51 ± 0.03	0.53 ± 0.03	0.48 ± 0.05	0.53 ± 0.05	0.53 ± 0.04	0.57 ± 0.02	0.58 ± 0.01
1614503	0.49 ± 0.03	0.51 ± 0.07	0.56 ± 0.06	0.70 ± 0.22	nan	0.49 ± 0.07	0.55 ± 0.05	0.59 ± 0.02	0.76 ± 0.22	nan
1614508	0.84 ± 0.02	0.85 ± 0.03	0.86 ± 0.03	0.89 ± 0.04	nan	0.86 ± 0.02	0.86 ± 0.02	0.87 ± 0.02	0.88 ± 0.04	nan
1614522	0.58 ± 0.04	0.61 ± 0.03	0.60 ± 0.03	0.64 ± 0.02	0.67 ± 0.03	0.58 ± 0.03	0.60 ± 0.03	0.61 ± 0.03	0.64 ± 0.02	0.67 ± 0.02
1737951	0.65 ± 0.08	0.71 ± 0.06	0.76 ± 0.04	0.80 ± 0.06	nan	0.63 ± 0.06	0.67 ± 0.05	0.71 ± 0.04	0.75 ± 0.07	nan
1738079	0.49 ± 0.03	0.49 ± 0.03	0.50 ± 0.04	0.49 ± 0.04	nan	0.49 ± 0.02	0.49 ± 0.03	0.50 ± 0.03	0.54 ± 0.06	nan
1738362	0.46 ± 0.06	0.55 ± 0.08	0.59 ± 0.06	0.64 ± 0.22	nan	0.49 ± 0.10	0.56 ± 0.09	0.65 ± 0.05	0.82 ± 0.17	nan

Table 9: MAML results measuring  $\Delta$ AUPRC on the first 50 tasks in the test set of FS-Mol.

TASK-ID	16 (IGNITE-MAML)	32 (IGNITE-MAML)	64 (IGNITE-MAML)	128 (IGNITE-MAML)	256 (IGNITE-MAML)	16 (MAML)	32 (MAML)	64 (MAML)	128 (MAML)	256 (MAML)
1006005	0.47 ± 0.03	0.49 ± 0.05	0.49 ± 0.04	0.54 ± 0.06	nan	0.49 ± 0.02	0.51 ± 0.04	0.52 ± 0.03	0.56 ± 0.05	nan
1066254	0.58 ± 0.07	0.61 ± 0.05	0.65 ± 0.07	0.65 ± 0.13	nan	0.56 ± 0.07	0.58 ± 0.04	0.59 ± 0.07	0.63 ± 0.15	nan
1119333	0.73 ± 0.03	0.74 ± 0.03	0.77 ± 0.04	0.76 ± 0.05	0.77 ± 0.06	0.70 ± 0.03	0.72 ± 0.04	0.74 ± 0.05	0.72 ± 0.02	0.74 ± 0.05
1243967	0.72 ± 0.03	0.76 ± 0.03	0.75 ± 0.04	0.77 ± 0.04	nan	0.72 ± 0.05	0.75 ± 0.01	0.74 ± 0.04	0.76 ± 0.04	nan
1243970	0.70 ± 0.04	0.71 ± 0.01	0.70 ± 0.02	0.71 ± 0.03	nan	0.71 ± 0.03	0.72 ± 0.03	0.72 ± 0.03	0.68 ± 0.03	nan
1613777	0.53 ± 0.01	0.53 ± 0.01	0.53 ± 0.01	0.54 ± 0.02	0.54 ± 0.02	0.50 ± 0.01	0.51 ± 0.01	0.51 ± 0.01	0.53 ± 0.02	0.53 ± 0.02
1613800	0.40 ± 0.00	0.40 ± 0.01	0.41 ± 0.01	0.42 ± 0.01	0.42 ± 0.01	0.40 ± 0.01	0.40 ± 0.01	0.40 ± 0.01	0.41 ± 0.01	0.41 ± 0.01
1613898	0.56 ± 0.02	0.55 ± 0.04	0.58 ± 0.04	0.57 ± 0.08	nan	0.57 ± 0.02	0.56 ± 0.03	0.56 ± 0.03	0.56 ± 0.04	nan
1613907	0.54 ± 0.03	0.55 ± 0.04	0.54 ± 0.06	0.55 ± 0.07	nan	0.53 ± 0.03	0.51 ± 0.02	0.53 ± 0.05	0.55 ± 0.13	nan
1613926	0.67 ± 0.04	0.65 ± 0.06	0.71 ± 0.06	0.78 ± 0.20	nan	0.57 ± 0.09	0.59 ± 0.10	0.65 ± 0.12	0.77 ± 0.12	nan
1613949	0.46 ± 0.04	0.47 ± 0.04	0.47 ± 0.05	0.45 ± 0.10	nan	0.48 ± 0.03	0.48 ± 0.04	0.48 ± 0.06	0.43 ± 0.09	nan
1614027	0.51 ± 0.02	0.52 ± 0.02	0.54 ± 0.02	0.57 ± 0.03	0.60 ± 0.02	0.52 ± 0.01	0.52 ± 0.01	0.53 ± 0.03	0.54 ± 0.03	0.58 ± 0.04
1614153	0.33 ± 0.01	0.34 ± 0.01	0.33 ± 0.01	0.34 ± 0.01	0.34 ± 0.01	0.33 ± 0.01	0.34 ± 0.01	0.34 ± 0.01	0.35 ± 0.01	0.36 ± 0.01
1614292	0.35 ± 0.02	0.36 ± 0.02	0.37 ± 0.02	0.37 ± 0.02	0.39 ± 0.01	0.35 ± 0.01	0.35 ± 0.01	0.35 ± 0.01	0.35 ± 0.01	0.35 ± 0.01
1614423	0.44 ± 0.07	0.52 ± 0.10	0.64 ± 0.03	0.69 ± 0.05	0.71 ± 0.04	0.45 ± 0.05	0.47 ± 0.07	0.51 ± 0.07	0.60 ± 0.07	0.68 ± 0.02
1614433	0.46 ± 0.02	0.46 ± 0.02	0.47 ± 0.02	0.49 ± 0.03	0.52 ± 0.04	0.44 ± 0.01	0.46 ± 0.03	0.47 ± 0.03	0.48 ± 0.04	0.49 ± 0.04
1614466	0.46 ± 0.01	0.46 ± 0.02	0.47 ± 0.02	0.47 ± 0.02	0.51 ± 0.03	0.47 ± 0.01	0.48 ± 0.02	0.49 ± 0.02	0.49 ± 0.02	0.51 ± 0.03
1614503	0.35 ± 0.04	0.36 ± 0.06	0.37 ± 0.04	0.56 ± 0.24	nan	0.37 ± 0.02	0.36 ± 0.03	0.38 ± 0.04	0.57 ± 0.20	nan
1614508	0.70 ± 0.12	0.77 ± 0.13	0.80 ± 0.05	0.82 ± 0.09	nan	0.66 ± 0.08	0.79 ± 0.07	0.77 ± 0.09	0.83 ± 0.09	nan
1614522	0.52 ± 0.05	0.53 ± 0.03	0.54 ± 0.06	0.61 ± 0.02	0.62 ± 0.02	0.50 ± 0.03	0.52 ± 0.02	0.52 ± 0.04	0.56 ± 0.03	0.58 ± 0.03
1737951	0.49 ± 0.09	0.46 ± 0.07	0.61 ± 0.03	0.67 ± 0.06	nan	0.57 ± 0.04	0.57 ± 0.03	0.58 ± 0.04	0.58 ± 0.07	nan
1738079	0.48 ± 0.01	0.47 ± 0.01	0.47 ± 0.02	0.49 ± 0.04	nan	0.52 ± 0.01	0.51 ± 0.01	0.51 ± 0.03	0.52 ± 0.03	nan
1738362	0.31 ± 0.03	0.34 ± 0.05	0.34 ± 0.07	0.64 ± 0.23	nan	0.37 ± 0.01	0.38 ± 0.03	0.40 ± 0.04	0.46 ± 0.19	nan
1738395	0.49 ± 0.03	0.50 ± 0.03	0.49 ± 0.03	0.50 ± 0.05	nan	0.50 ± 0.03	0.48 ± 0.03	0.48 ± 0.03	0.50 ± 0.05	nan
1738485	0.49 ± 0.01	0.51 ± 0.02	0.52 ± 0.04	0.54 ± 0.04	0.55 ± 0.06	0.49 ± 0.01	0.49 ± 0.01	0.48 ± 0.01	0.50 ± 0.06	0.54 ± 0.06
1738502	0.39 ± 0.01	0.40 ± 0.02	0.40 ± 0.02	0.43 ± 0.04	0.43 ± 0.04	0.41 ± 0.01	0.42 ± 0.02	0.41 ± 0.02	0.41 ± 0.02	0.41 ± 0.02
1738573	0.51 ± 0.02	0.50 ± 0.01	0.51 ± 0.02	0.52 ± 0.02	0.53 ± 0.02	0.52 ± 0.01	0.51 ± 0.01	0.52 ± 0.01	0.52 ± 0.01	0.52 ± 0.01
1738579	0.54 ± 0.03	0.56 ± 0.02	0.56 ± 0.03	0.60 ± 0.05	nan	0.53 ± 0.03	0.55 ± 0.03	0.55 ± 0.04	0.58 ± 0.04	nan
1738633	0.55 ± 0.04	0.56 ± 0.04	0.60 ± 0.04	0.57 ± 0.09	nan	0.59 ± 0.02	0.60 ± 0.02	0.60 ± 0.04	0.63 ± 0.12	nan
1794324	0.52 ± 0.02	0.52 ± 0.01	0.52 ± 0.01	0.53 ± 0.02	0.54 ± 0.02	0.51 ± 0.00	0.51 ± 0.01	0.52 ± 0.01	0.52 ± 0.01	0.53 ± 0.01
1794504	0.68 ± 0.01	0.70 ± 0.04	0.71 ± 0.04	0.85 ± 0.24	nan	0.65 ± 0.05	0.66 ± 0.05	0.71 ± 0.04	0.85 ± 0.24	nan
1794519	0.64 ± 0.05	0.66 ± 0.07	0.69 ± 0.08	0.73 ± 0.13	nan	0.64 ± 0.07	0.62 ± 0.05	0.65 ± 0.07	0.71 ± 0.11	nan
1794557	0.53 ± 0.02	0.54 ± 0.01	0.54 ± 0.02	0.53 ± 0.02	0.53 ± 0.01	0.55 ± 0.01	0.55 ± 0.01	0.55 ± 0.01	0.55 ± 0.01	0.55 ± 0.01
1963701	0.60 ± 0.01	0.59 ± 0.02	0.59 ± 0.02	0.60 ± 0.01	0.60 ± 0.02	0.60 ± 0.01	0.59 ± 0.01	0.59 ± 0.01	0.59 ± 0.01	0.59 ± 0.02
1963705	0.71 ± 0.03	0.70 ± 0.02	0.72 ± 0.01	0.72 ± 0.01	0.71 ± 0.02	0.77 ± 0.01	0.77 ± 0.02	0.77 ± 0.01	0.77 ± 0.03	0.76 ± 0.04
1963715	0.63 ± 0.00	0.62 ± 0.03	0.63 ± 0.01	0.64 ± 0.01	0.64 ± 0.02	0.63 ± 0.01	0.61 ± 0.04	0.64 ± 0.01	0.64 ± 0.01	0.64 ± 0.02
1963721	0.50 ± 0.02	0.50 ± 0.02	0.50 ± 0.02	0.51 ± 0.04	0.55 ± 0.07	0.52 ± 0.02	0.51 ± 0.01	0.52 ± 0.01	0.51 ± 0.03	0.54 ± 0.09
1963723	0.72 ± 0.03	0.73 ± 0.01	0.73 ± 0.01	0.74 ± 0.02	0.75 ± 0.02	0.72 ± 0.03	0.74 ± 0.02	0.74 ± 0.01	0.75 ± 0.02	0.77 ± 0.02
1963731	0.70 ± 0.02	0.70 ± 0.01	0.70 ± 0.02	0.76 ± 0.06	0.76 ± 0.05	0.71 ± 0.03	0.74 ± 0.02	0.74 ± 0.02	0.76 ± 0.02	0.79 ± 0.03
1963741	0.65 ± 0.02	0.66 ± 0.00	0.66 ± 0.01	0.67 ± 0.01	0.67 ± 0.01	0.65 ± 0.01	0.65 ± 0.01	0.66 ± 0.01	0.65 ± 0.01	0.65 ± 0.01
1963756	0.76 ± 0.05	0.75 ± 0.04	0.76 ± 0.04	0.77 ± 0.02	0.77 ± 0.01	0.71 ± 0.02	0.72 ± 0.03	0.70 ± 0.04	0.72 ± 0.02	0.72 ± 0.03
1963773	0.60 ± 0.01	0.59 ± 0.04	0.60 ± 0.03	0.60 ± 0.02	0.60 ± 0.02	0.62 ± 0.02	0.63 ± 0.02	0.63 ± 0.02	0.64 ± 0.03	0.63 ± 0.02
1963799	0.63 ± 0.01	0.62 ± 0.01	0.61 ± 0.03	0.61 ± 0.02	0.60 ± 0.05	0.64 ± 0.02	0.66 ± 0.01	0.66 ± 0.02	0.67 ± 0.03	0.67 ± 0.07
1963810	0.78 ± 0.01	0.77 ± 0.02	0.78 ± 0.01	0.78 ± 0.01	0.78 ± 0.01	0.77 ± 0.01	0.75 ± 0.03	0.76 ± 0.02	0.76 ± 0.02	0.78 ± 0.02
1963818	0.71 ± 0.02	0.72 ± 0.01	0.72 ± 0.03	0.73 ± 0.02	0.73 ± 0.03	0.70 ± 0.04	0.72 ± 0.01	0.72 ± 0.03	0.72 ± 0.03	0.73 ± 0.03
1963819	0.59 ± 0.04	0.61 ± 0.03	0.59 ± 0.01	0.61 ± 0.03	0.61 ± 0.03	0.60 ± 0.02	0.61 ± 0.03	0.62 ± 0.03	0.63 ± 0.04	0.63 ± 0.03
1963824	0.62 ± 0.04	0.63 ± 0.02	0.65 ± 0.04	0.65 ± 0.04	0.69 ± 0.05	0.62 ± 0.03	0.64 ± 0.04	0.64 ± 0.04	0.63 ± 0.03	0.63 ± 0.04
1963825	0.73 ± 0.01	0.72 ± 0.02	0.73 ± 0.01	0.74 ± 0.02	0.75 ± 0.04	0.77 ± 0.02	0.77 ± 0.02	0.79 ± 0.02	0.79 ± 0.03	0.80 ± 0.04
1963827	0.78 ± 0.03	0.80 ± 0.01	0.80 ± 0.03	0.79 ± 0.02	0.80 ± 0.02	0.78 ± 0.01	0.76 ± 0.04	0.76 ± 0.03	0.77 ± 0.01	0.76 ± 0.02
1963831	0.69 ± 0.01	0.69 ± 0.02	0.69 ± 0.01	0.69 ± 0.02	0.68 ± 0.06	0.68 ± 0.02	0.68 ± 0.02	0.70 ± 0.02	0.71 ± 0.03	0.72 ± 0.05
1963838	0.49 ± 0.01	0.49 ± 0.01	0.51 ± 0.04	0.55 ± 0.03	nan	0.54 ± 0.02	0.53 ± 0.01	0.55 ± 0.02	0.52 ± 0.04	nan